Electron tomography of molecules and cells

Wolfgang Baumeister, Rudo Grimm and Jochen Walz

Electron tomography is the most widely applicable method for obtaining three-dimensional information by electron microscopy. It is, in fact, the only method suitable for investigating pleomorphic structures, such as many supramolecular assemblies, organelles and cells. With the recent development of automated low-dose data-acquisition schemes, it is now possible to study molecules and cells embedded in vitreous ice. This opens up new horizons for investigating the functional organization of cellular components with minimal perturbation of the cellular context.

Electron tomography is by no means a new imaging technology, but it has only gained momentum in recent years. Three decades ago, R. G. Hart published a remarkable paper entitled: Electron microscopy of unstained biological material: The polytropic montage[1]. The abstract reads as follows: 'With use of an electronic picture-scanning device and a digital computer, electron micrographs taken of a specimen along several different directions can be superimposed to form a montage that is more informative than the component images. Preliminary results indicate that one may thus study unstained, unshadowed biological material at high resolution.' Despite its vision, the Hart paper had negligible impact and was largely forgotten. For a vision to materialize, timing is a crucial element: if it is too early, the necessary technologies might not yet exist.

In the same year, 1968, another paper was published that, in retrospect, is seen as the landmark paper in biomolecular electron microscopy. De Rosier and Klug[2] outlined very clearly and in general terms the principles of three-dimensional (3-D) reconstruction. Realizing the practical problems in recording 3-D data sets, they took advantage of symmetry in a very pragmatic manner. With helical structures, a single projection contains all the necessary information, and this allowed them to obtain a 3-D reconstruction of a negatively stained bacteriophage T4 tail. In 1974, Taylor and Glaeser[3] made an important observation that in the following years changed specimen preparation radically: catalase microcrystals, kept in a frozen-hydrated state, yielded electron diffraction patterns extending in resolution to 0.3 nm. Another milestone was the work on purple membrane by Unwin and Henderson[4,5], which demonstrated that high-resolution images can be obtained with glucose-embedded samples, provided the data are recorded under low-dose conditions and the signals are retrieved by extensive image averaging. Their work paved the way for the now-evident success of electron crystallography – with good enough two-dimensional crystals, near-atomic resolution is attainable.

Back in 1968, W. Hoppe, guided by his background in x-ray crystallography, also realized the potential of three-dimensional electron microscopy[6]. Diverging from other approaches, he focused on the development of methods suitable for studying individual structures, and, as early as 1974, his group presented a 3-D reconstruction of a single fatty acid synthetase molecule obtained by electron tomography[7]. The 'brute force' approach provoked some criticism[8] – besides doubts that negative staining can portray fine details of structures accurately enough, the main concern was the enormous electron dose to which the specimen was exposed while recording the 3-D data set. There was much discussion in the following years of whether it might eventually be possible to do electron tomography with 'molecular resolution' at acceptable electron doses (e.g. see Refs 9–11).

Problems in electron tomography

The basic principle of electron tomography is illustrated in Fig. 1 and described in the corresponding legend. Electron tomography is in fact the most widely applicable approach for obtaining 3-D information by electron microscopy. It can depict unique structures and scenes, but an implication of this is that it cannot take advantage of image-averaging techniques for noise reduction.

The key problem in electron tomography is reconciling two requirements that are in conflict with one another: to obtain an undistorted and detailed reconstruction, one has to collect data over as wide a tilt range as possible with increments as small as possible (see Fig. 1). At the same time, the electron dose must be minimized. Above a critical dose, the specimen undergoes structural degradation that, in the worst case, renders reconstructions meaningless. In principle, one can fractionate the dose evenly over as many projections as an optimized tilt geometry allows; however, the signal-to-noise ratio will deteriorate and the alignment eventually becomes unreliable. This problem is aggravated by the limited mechanical accuracy of specimen holders; deviations from ideal tilt geometry (owing to nonperfect eucentricity, instability and drift of the specimen holder) cause movements in the x-, y- and z-directions that translate into lateral shifts and changes of focus. Therefore, following each change of tilt angle, the specimen (or image) has to be realigned and refocused. This can be done manually – but at the expense of additional exposure of the specimen to the

The authors are in the Max-Planck-Institut für Biochemie, Abteilung Molekulare Strukturbiologie, Am Klopferspitz 18a, 82152 Martinsried, Germany. E-mail: baumeist@biochem.mpg.de

0962-8924/99/$ – see front matter

PII: S0962-8924(98)01423-8

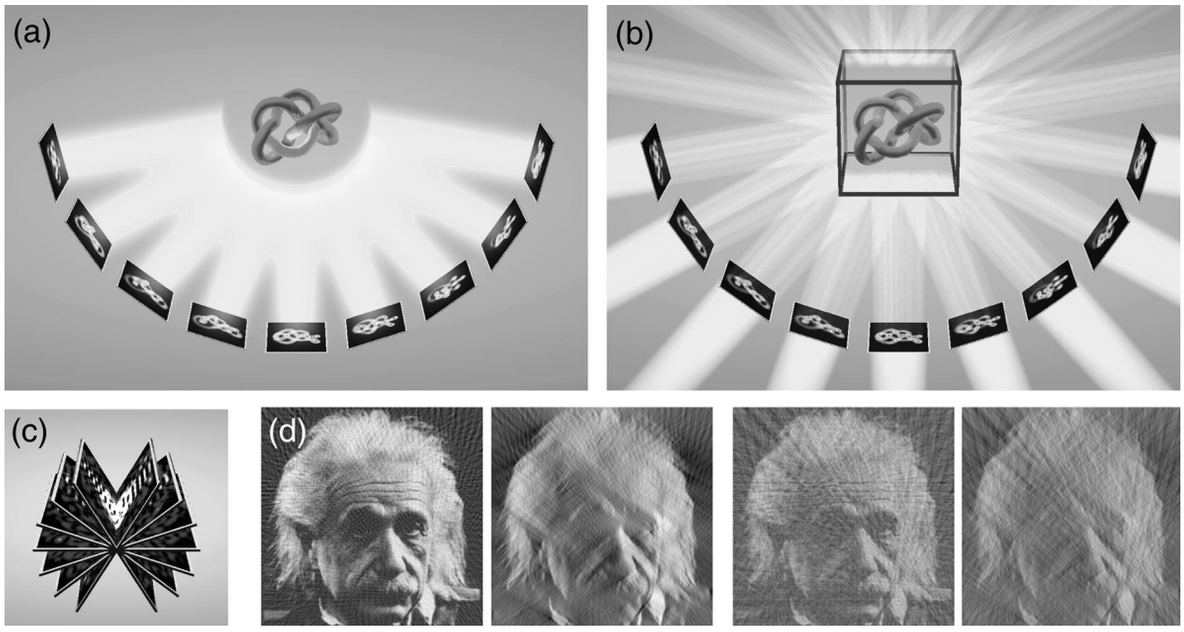

FIGURE 1

(a) The three-dimensional (3-D) reconstruction of an object from a series of projections is commonly referred to as tomography. The figure shows a single axis tilt series data-acquisition scheme. A set of 2-D projection images is recorded while tilting either the object or illumination and detector incrementally around one axis. (b) The backprojection method helps to explain the principle of 3-D reconstruction in a fairly intuitive manner: for each projection, a backprojection body is calculated, and the sum of all the backprojection bodies represents the density distribution of the original object. To compensate for features that are present in two or more projections, an appropriate weighting function has to be applied to the 2-D images before calculating the reconstruction (for details, see Refs 38 and 39). (c) By transposing the principle of tomography to Fourier space, some of the problems become obvious: each projection in real space is represented by a central section. When a limited number of images is recorded with relatively large tilt increments, the Fourier space is sampled incompletely at higher frequencies, thus limiting the isotropic resolution. Moreover, the specimen cannot be tilted to $\pm 90°$ because of technical constraints. The absence of data in a wedge-shaped region causes various kinds of distortions in the reconstructed volume known as 'missing-wedge artifacts'. (d) The four panels illustrate the effects of tilt increments and tilt range on the quality of the reconstruction. Reconstructions of a 2-D image from different sets of 1-D projections simulate an x–z-slice of a 3-D object. The first image (left) shows a nearly perfect reconstruction obtained with a $\pm 90°$ tilt range and 2° tilt increment. In calculating the second image, the tilt range was restricted to $\pm 60°$. Owing to the missing wedge, the image details perpendicular to the virtual z-direction are smeared out. The two images on the right were reconstructed with tilt increments of 5° and tilt ranges of $\pm 90°$ and $\pm 60°$, respectively. Compared with the first two images, the resolution is lower, and the images are more degraded.

beam. In fact, the dose 'overhead' spent on these realignments can far exceed the dose spent 'usefully' on recording data.

Automated electron tomography

With the advent of computer-controlled transmission electron microscopes (Fig. 2) and the availability of large-area charge-coupled device (CCD) cameras, it became possible to implement complex image-acquisition schemes running in a fully automated fashion[12,13]. This not only made the recording of tomographic data sets much less cumbersome but also made it possible to minimize the exposure of the specimen to the electron beam. At lower magnifications, suitable for imaging large-scale structures at a resolution of ~5 nm, data sets comprising up to 150 projections can be recorded with a cumulative dose as low as 5000 $e^{-}nm^{-2}$; at higher magnifications and with resolution targets in the 2 nm range, one aims not to exceed a dose of 2000 $e^{-}nm^{-2}$. The fraction of the dose that is spent as overhead [search, recentering, (auto)focusing] can be kept as low as 3% of the total; in other words, almost all electrons are used to retrieve information. This has changed the perspectives of electron tomography quite dramatically – it is now possible to analyse specimens embedded in vitreous ice[14] as demonstrated with lipid vesicles and vesicles loaded with actin filaments[15,16]. Thus, not only are all the adverse effects of fixation, staining and plastic embedding avoided, but it is now possible to aim at capturing the dynamic events occurring in cells or supramolecular assemblies under near-physiological conditions.

Electron tomography of molecular structures

Today, electron tomography is capable of analysing the structure of individual macromolecules with resolutions in the 2 nm range (e.g. see Fig. 3). In many cases, this is sufficient to fit high-resolution structures of subunits or domains obtained by x-ray crystallography or NMR spectroscopy into envelopes of the electron tomographic maps. The composite models bridge the resolution gap and provide insights into macromolecular interactions or into conformational states that cannot otherwise be captured. Electron tomography can also provide reliable starting models of molecular structures, which can then be refined iteratively: by reprojecting such an initial model, 'virtual' tilt angles can be assigned to projection data, which can

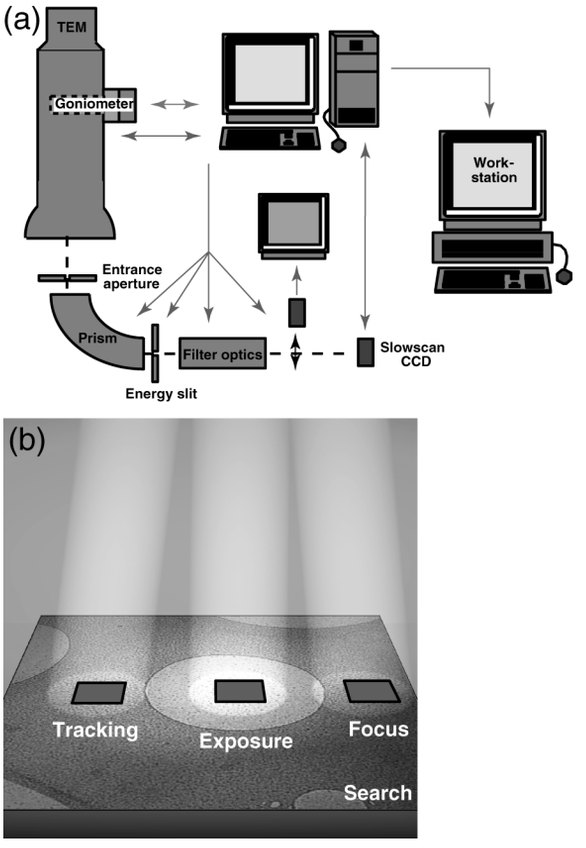

FIGURE 2

(a) The setup for electron tomographic data acquisition consists of a computer-controlled transmission electron microscope (TEM) equipped with a eucentric goniometer. An energy filter can be added optionally to remove inelastically scattered electrons; the resulting improvement in image quality is particularly important when investigating biological specimens with a thickness equal to or larger than the mean free path length of electrons (about 200 nm for 120 kV acceleration voltage). Data are recorded with a cooled slow-scan charge-coupled device (CCD) camera, a detection device with high sensitivity and linearity. Owing to the mechanical imperfections of specimen holders, in particular cryoholders, the specimen is displaced from its original position upon tilting, resulting in image shifts and changes of focus. Displacements can accumulate to several microns in recording a full tilt series. Therefore, at typical magnifications of 10 000× to 60 000×, the specimen area under investigation might completely disappear from the restricted field of view of the CCD camera. However, since the data recorded with the CCD camera are instantly available in digital format, image shifts can be measured online by cross-correlation when setting a new tilt angle. Focal changes are determined and corrected using an autofocus procedure. Taking the advantage of computer control of the TEM, deflection coils and objective lens current can be adjusted to correct for image displacements and for changes of focus. Once the acquisition of a tilt series is complete, the data are transferred to a workstation via ethernet for fine tuning of the alignments and for three-dimensional (3-D) reconstruction. (b) Biological specimens are sensitive to irradiation with high-energy electrons. The cumulative dose for imaging in 3-D must not exceed a critical dose of ~1000 to 2000 $e^{-}nm^{-2}$ for depicting high-resolution features, or 10 000 $e^{-}nm^{-2}$ for a medium resolution. Since manual correction of the specimen shifts during acquisition of a tilt series is almost impossible under low-dose conditions, automated procedures are used for data acquisition. The figure shows the low-dose image-acquisition scheme used in automated electron tomography. In a first step, an image is recorded at low magnification with low-intensity illumination to obtain an overview (Search area). This image is subsequently used for a coarse correction of the image shift with respect to the position at the previous tilt angle. The TEM is then switched to high magnification (e.g. 30 000×), shifting the beam to the Focus area. At this area, the images required for focus determination are recorded. After focus correction, the beam is shifted to the Tracking area, where the fine correction for the image shift takes place. Finally, the projection of the tilt series is recorded at the Exposure area. The procedures are repeated for each tilting step. Even if the Focus and Tracking area are identical to the Exposure area in a simpler data-acquisition scheme, most of the dose (>80%) is used for recording the final projection when working with an automated setup as shown in (a). The dose for each projection can be kept as low as 100 $e^{-}nm^{-2}$. Typically, tilt series with 20–40 projections are recorded with ice-embedded molecular specimens. For larger-scale structures and lower-resolution targets, the acquisition of more than 150 projections from one specimen area is feasible without exceeding the allowable dose. If data were recorded manually, most of the dose would be spent as an 'overhead' for tracking the specimen and adjusting focus. This would lead to intolerably high exposures and thus to massive radiation damage.

be recorded conventionally at very low doses. Recently, such a hybrid approach has been used to determine the structure of Tricorn protease capsids[17]. The icosahedral structure was established by electron tomography, and, by exploiting the symmetry, a refined structure was calculated from projection data. The tomographic approach has distinct advantages when a population of molecules displays substantial variances. The 3-D reconstructions of individual molecules can be subjected to multivariate statistical analysis to generate class averages representing different conformational states and states of association, for example.

If the population of macromolecules under scrutiny is structurally homogeneous, methods that are philosophically akin to electron tomography can be used. Two such 'quasi-tomographic' approaches referred to as 'random conical tilting' and 'angular reconstitution' are in use, which were pioneered by the groups of J. Frank[18] and M. van Heel[19], respectively. Neither method requires the recording of tilt series; instead, they make use of the manifold orientations of nearly identical copies of a macromolecule present in a single image to generate a 'virtual' set of tilted projections. Many particles assume a preferred orientation when adsorbed to a carbon film, except for in-plane rotations. Therefore, the particle projections in a single tilted image correspond to a conical tilt series with a random distribution of the projection vectors on the cone[18]. Angular reconstitution relies on a random orientation of particles, as is often observed when macromolecules are embedded in an unsupported ice layer. Projection vectors have to be assigned *a posteriori* to the projections present in a single image[19]; ideally, they cover the complete angular range. Compared with electron tomography *sensu strictu*, the data acquisition is straightforward, and the total dose can be spent on a single image. Obviously, the much higher contrast of such images facilitates an

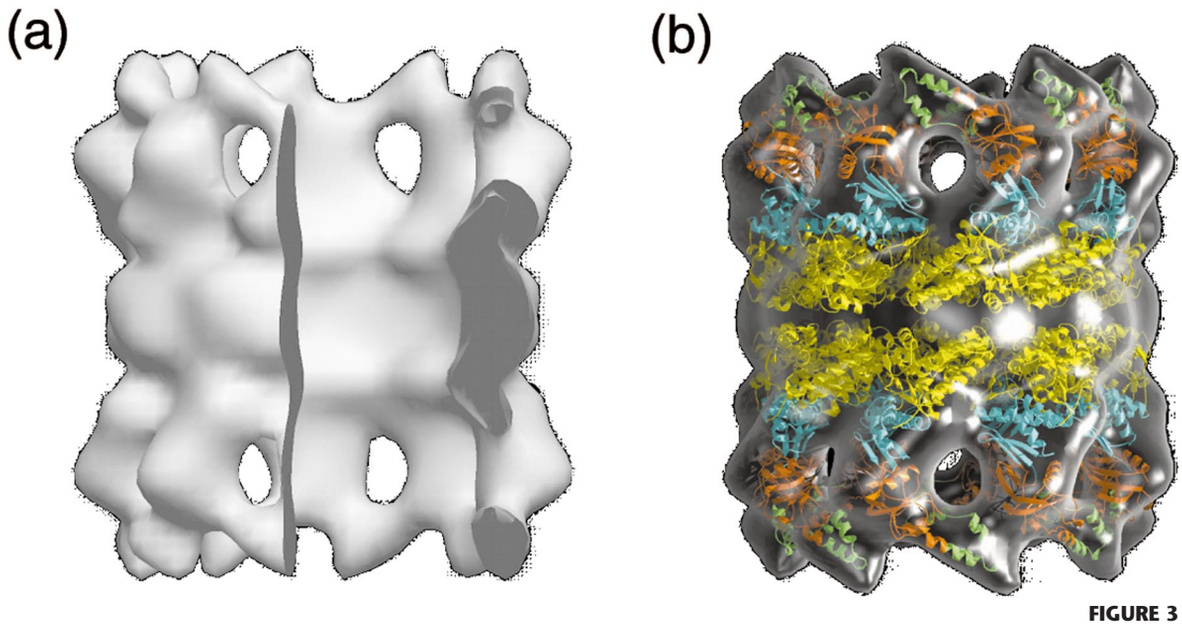

FIGURE 3

Three-dimensional map of the thermosome obtained by cryoelectron tomography. The thermosome is the archetype of the group II chaperonins, which, besides the archaeal members, also comprise the chaperonins of the cytosol of eukaryotes, known as TRiC or CCT (for a recent review, see Ref. 40). Thermosomes embedded in ice were reconstructed individually, before the data set was subjected to three-dimensional (3-D) alignment, classification and averaging. The map shown in (a) is calculated from 227 particles; the tilt increments were 6° and the effective tilt range was ±65°. The cumulative dose for recording the whole data set was ~2000 $e^{-}nm^{-2}$. The reconstruction was low-pass filtered with a cut-off at $(2.8\ nm)^{-2}$. The thermosome is depicted in the open – i.e. substrate accepting – conformation. A 90° segment was removed to provide a view of the interior of the complex. (b) Tomographic map in a transparent representation with crystal structures of the domains fitted into it. The equatorial domains are shown in yellow, the intermediate domains in blue and the apical domains in orange (base) and green (apical or lid subdomain; for details, see Ref. 41). The open thermosome has a diameter of ~15 nm and a height of ~18 nm. By combining the low-resolution tomographic map with the high-resolution domain structures, the resolution gap is bridged and pseudo-atomic structures are obtained. Thus, detailed pictures of molecular assemblies or of conformational states can be obtained that are difficult to capture or preserve in crystallization experiments.

accurate alignment, which ultimately determines resolution. Structural studies with *Escherichia coli* ribosomes[20,21] or the ryanodine receptor[22,23] ('Ca^{2+}-release channel') have clearly demonstrated that these approaches provide reliable structural information at 2 nm resolution and beyond. In principle, it should be possible to attain subnanometer resolutions with these elegant methods[24], and in fact this goal has already been achieved with large symmetric particles such as hepatitis B virus core particles[25,26].

Electron tomography of cellular structures

Until recently, there were few applications of electron tomography in cell biology. This reflects, not least, the practical problems encountered when data sets are recorded manually. Also, even with plastic-embedded materials, radiation damage poses a serious problem. Sections can shrink in thickness by as much as 35%[27]. Cooling of the sample to the temperature of liquid nitrogen is helpful but does not eliminate the problem altogether. Nevertheless, some spectacular insights into cellular organization have been obtained by electron tomography of thick sections. Examples are the organization of the Golgi apparatus[28], or the endoplasmic[29] reticulum, as well as structural studies of mitochondria[30,31] and centrosomes[32].

Automated electron tomography in a low-dose regime allows the investigation of unfixed and unstained cellular structures embedded in vitreous ice. This guarantees not only a lifelike preservation of the cell but also avoids the problems that arise in interpreting density patterns resulting from poorly understood interactions between structure and stain. Fig. 4 shows two slices, each about the thickness of a single macromolecule (12 nm) through a tomographic reconstruction of a whole archaebacterium embedded in ice. The wealth of structural features seen in these slices is striking, and some of the features were unexpected. There are indications of more membrane dynamics than anticipated, including various forms of vesicle traffic across the cell envelope. The resolution is still modest (5–7 nm), but there is room for improvement – even with existing technologies, it should be possible to improve resolution by a factor of two to three. This would be sufficient to bring it into the realm of 'molecular resolution', enabling recognition of larger individual macromolecules by their size and shape[33].

The crowded nature of the cytosol and the noise level in such reconstructions mean that the identification of molecular species based on visual inspection might not be a realistic goal. The application of existing noise-reduction techniques optimized for electron tomography can be quite helpful in visualizing and interpreting larger-scale structures (membranes, filaments) in such volume data[34] but provides only little assistance in detecting single molecules. The identification of a given molecule in a volume could be based on 3-D correlation or on sophisticated pattern-recognition techniques; a 3-D cross-correlation peak might be significant even if the particle is barely recognizable. Suitable templates

can be derived from data obtained with high-resolution techniques (NMR spectroscopy, x-ray and electron crystallography) and used for searching reconstructed volumes. This will allow mapping of the spatial distribution of molecules and the identification of molecular interactions with minimal perturbations of the cellular context. Examples of the sort of questions that could be addressed include: what portion of 20S proteasomes is associated with 19S regulatory complexes, and where are they located, or what are the spatial relationships between chaperonins and proteasomes. Electron tomography of frozen-hydrated cells is basically a non-invasive method that has great potential for studying the functional organization of cellular components.

Unfortunately, the specimen thickness that can be imaged with electron tomography is limited. The fraction of inelastically scattered electrons increases with specimen thickness, causing a blurring of the images. Energy filtering improves the situation by removing the 'inelastic background'. Furthermore, the tilt increment has to be lowered with increasing thickness in order to obtain a reconstruction with a certain target resolution; in practice, more images result in higher cumulative electron doses. For a medium-voltage transmission electron microscope (300 kV) equipped with an energy filter, the maximum specimen thickness for which molecular resolution is achievable is estimated to be about 0.5 microns[35]. While this still allows investigation of prokaryotic cells *in toto*, larger structures have to be examined in the form of cryosections; in conjunction with high-pressure freezing, this technique minimizes structural perturbations[36].

Blueprint for the future

With continuing technical developments, we can expect that, over the next few years, electron tomography will reveal structures of unprecedented complexity and major biological significance. There is a growing awareness that cells are not merely a collection of freely diffusing and randomly colliding individual molecules[37]; molecules assemble to form molecular machines, and the coordinate operation of many such machines with specialized tasks makes the cell a factory. Electron tomography provides insights into the organization of the cell factory and, in conjunction with high-resolution techniques, blueprints of the machines. Not being constrained by crystal lattices, these machines can be studied in action.

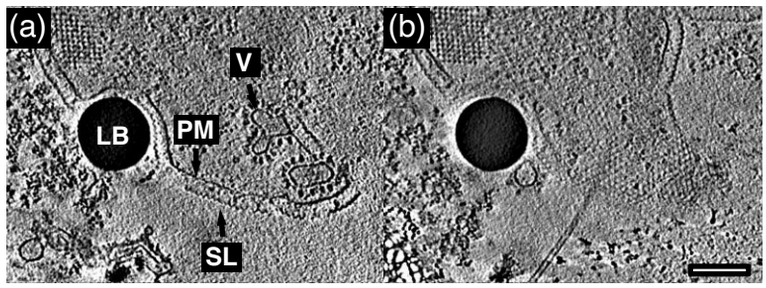

FIGURE 4

Electron tomographic reconstruction of a whole cell of the archaebacterium *Pyrodictium abyssi* embedded in vitreous ice. (a, b) Two 12-nm thick slices through the reconstructed volume; the distance between the two slices is ~90 nm. Cells were taken from a growing culture, transferred to a carbon film with large holes and shock frozen. Tomographic data sets of 100 to 150 projections with tilt angles spaced in proportion to cos ψ and covering an angular range from –68° to +62° were recorded of cells in ~250-nm thick ice across the holes. The cumulative dose was between 5000 and 7000 $e^{-}nm^{-2}$. The regular surface layer (SL), which forms a porous canopy 40 nm above the surface of the plasma membrane (PM), is clearly visible at the periphery of the cell. Where the slices are nearly parallel to the S-layer plane, the periodicity of ~21 nm is discernible. Jointly, the S-layer and the plasma membrane delimit a 'quasi-periplasmic space'[42]. The cell appears to be in the process of engulfing a latex bead (LB) of diameter 250 nm. Inside the cell, a small protein crystal (lattice spacing 17.7 nm) and several vesicles (V) are clearly visible. Some of these vesicles are docked to the plasma membrane and have recruited an array of particles on their outer surface. The existence of such vesicles and of vesicle traffic across the cell wall were quite unexpected findings. Bar, 200 nm.

References

1 Hart, R. G. (1968) *Science* 159, 1464–1467
2 De Rosier, D. J. and Klug, A. (1968) *Nature* 217, 130–134
3 Taylor, K. A. and Glaeser, R. M. (1974) *Science* 186, 1036–1038
4 Unwin, P. N. T. and Henderson, R. (1975) *J. Mol. Biol.* 94, 425–440
5 Henderson, R. and Unwin, P. N. T. (1975) *Nature* 257, 28–32
6 Hoppe, W. *et al.* (1968) *Naturwissenschaften* 7, 333–336
7 Hoppe, W. *et al.* (1974) *Hoppe-Seyler's Z. Physiol. Chem.* 355, 1483–1487
8 Baumeister, W. and Hahn, M. (1975) *Hoppe-Seyler's Z. Physiol. Chem.* 356, 1313–1316
9 Hegerl, R. and Hoppe, W. (1976) *Z. Naturforsch.* 31a, 1717–1721
10 Saxberg, B. E. H. and Saxton, W. O. (1981) *Ultramicroscopy* 6, 85–90
11 McEwen, B. F., Downing, K. H. and Glaser, R. M. (1995) *Ultramicroscopy* 60, 357–373
12 Dierksen, K. *et al.* (1992) *Ultramicroscopy* 40, 71–87
13 Dierksen, K. *et al.* (1993) *Ultramicroscopy* 49, 109–120
14 Dubochet, J. *et al.* (1988) *Quart. Rev. Biophys.* 21, 129–228
15 Dierksen, K. *et al.* (1995) *Biophys. J.* 68, 1416–1422
16 Grimm, R. *et al.* (1997) *Biophys. J.* 72, 482–489
17 Walz, J. *et al.* (1997) *Mol. Cell* 1, 59–65
18 Radermacher, M. *et al.* (1987) *J. Microsc.* 146, 113–136
19 van Heel, M. (1987) *Ultramicroscopy* 21, 111–124
20 Frank, J. *et al.* (1995) *Nature* 376, 441–444
21 Stark, H. *et al.* (1997) *Cell* 88, 19–28
22 Radermacher, M. *et al.* (1994) *J. Cell Biol.* 127, 411–423
23 Serysheva, I. I. *et al.* (1995) *Nat. Struct. Biol.* 2, 18–23
24 Henderson, R. (1995) *Quart. Rev. Biophys.* 28, 171–193
25 Böttcher, B., Wynne, S. A. and Crowther, R. A. (1997) *Nature* 386, 88–91
26 Conway, J. F. *et al.* (1997) *Nature* 386, 91–94
27 Luther, P. K., Lawrence, M. C. and Crowther, R. A. (1988) *Ultramicroscopy* 24, 7–18
28 Ladinsky, M. S. *et al.* (1994) *J. Cell Biol.* 127, 29–38
29 Martone, M. *et al.* (1993) *J. Neurosci.* 13, 4636–4646
30 Perkins, G. *et al.* (1997) *J. Struct. Biol.* 119, 260–272
31 Mannella, C. A. *et al.* (1994) *Microsc. Res. Tech.* 27, 278–283
32 Moritz, M. *et al.* (1995) *Nature* 378, 638–640
33 Koster, A. J. *et al.* (1997) *J. Struct. Biol.* 120, 276–308
34 Stoschek, A. and Hegerl, R. (1997) *J. Struct. Biol.* 120, 257–265
35 Grimm, R. *et al.* (1998) *Biophys. J.* 74, 1031–1042
36 Michel, M., Hillmann, T. and Müller, M. (1991) *J. Microsc.* 163, 3–18
37 Alberts, B. (1998) *Cell* 92, 291–294
38 Harauz, G. and van Heel, M. (1986) *Optik* 73, 146–156
39 Radermacher, M. *et al.* (1986) *J. Microsc.* 141, RP1
40 Klumpp, M. and Baumeister, W. (1998) *FEBS Lett.* 430, 73–77
41 Nitsch, M. *et al.* (1998) *Nat. Struct. Biol.* 5, 855–857
42 Wildhaber, I. and Baumeister, W. (1987) *EMBO J.* 6, 1475–1480

Acknowledgements

We are grateful to A. C. Steven for critical reading of the manuscript. This work was supported by grants from the Deutsche Forschungsgemeinschaft and a grant from the EU (BIO4-CT96-0099).